

Axisymmetric and stationary structures of magnetized barotropic stars with extremely strong magnetic fields deep inside

Kotaro Fujisawa ^{*}, Shin'ichirou Yoshida and Yoshiharu Eriguchi

Department of Earth Science and Astronomy, Graduate School of Arts and Sciences, University of Tokyo, Komaba, Meguro-ku, Tokyo 153-8902, Japan

Accepted 2012 January 23. Received 2012 January 23; in original form 2010 October 30

ABSTRACT

We have succeeded in obtaining magnetized star models that have extremely strong magnetic fields in the interior of the stars. In our formulation, arbitrary functions of the magnetic flux function appear in the expression of the current density. By appropriately choosing the functional form for one of the arbitrary functions which corresponds to the distribution of the *toroidal* current density, we have obtained configurations with magnetic field distributions that are highly localized within the central part and near the magnetic axis region. The absolute values of the central magnetic fields are stronger than those of the surface region by two orders of magnitude. By applying our results to magnetars, the internal magnetic *poloidal* fields could be 10^{17} G, although the surface magnetic fields are about 10^{15} G in the case of magnetars. For white dwarfs, the internal magnetic *poloidal* fields could be 10^{12} G, when the surface magnetic fields are $10^9 - 10^{10}$ G.

Key words: stars: magnetic field – stars: neutron – stars: white dwarf

1 INTRODUCTION

The magnetic field inside a star is scarcely detectable by direct observations but has been considered to affect stellar evolutions and activities in many aspects. For instance, if strong magnetic fields are hidden inside degenerate stars such as white dwarfs or neutron stars, they may significantly affect the cooling process of the stars by providing an energy reservoir or by modifying heat conduction. Highly localized, anisotropic and relatively strong magnetic field configurations, on the other hand, may affect accretion modes onto degenerate stars in close binary systems by providing a well-focused channel of accretion to their magnetic poles. In order to know the possible distributions and strengths of the magnetic fields inside the stars, we have to rely on theoretical studies. Until very recently, however, theoretical investigations could give us few hints about the interior magnetic fields. The reason for that may be twofold: one is related to the difficulty of the evolutionary computations of stellar magnetic fields and the other is related to the lack of methods to obtain stationary configurations of the magnetized stars.

Concerning the evolution of the stellar magnetic fields, since it has been very difficult to pursue evolutionary com-

putations of the global magnetic fields for both interiors and exteriors of stars, few results have been obtained. Recently, however, Braithwaite and his collaborators have succeeded in following the evolution of global stellar magnetic fields (Braithwaite & Spruit 2004; Braithwaite & Nordlund 2006; Braithwaite & Spruit 2006; Braithwaite 2006; Braithwaite 2007; Braithwaite 2008; Braithwaite 2009; Duez et al. 2010). They found that the twisted-torus configurations of the magnetic fields inside stars seem to be stable across the dynamical timescale.

On the other hand, to investigate possible structures of the interior and exterior magnetic fields by imposing stationarity is a different theoretical approach. Concerning this problem, many attempts have been made but it has also been difficult to obtain stellar structures with both *poloidal* and *toroidal* non force-free magnetic fields self-consistently, not only in the Newtonian gravity but also in general relativity (see e.g. Chandrasekhar & Fermi 1953; Ferraro 1954; Chandrasekhar 1956; Chandrasekhar & Prendergast 1956; Prendergast 1956; Woltjer 1959a; Woltjer 1959b; Woltjer 1960; Wentzel 1961; Ostriker & Hartwick 1968; Mikić 1973; Mikić 1975; Bocquet et al. 1995; Ioka & Sasaki 2004; Kiuchi & Yoshida 2008; Haskell et al. 2008; Duez & Mathis 2010). It is only recently that axisymmetric and stationary barotropic stellar structures have been successfully solved for configu-

* E-mail: fujisawa@ea.c.u-tokyo.ac.jp

rations with both *poloidal* and *toroidal* magnetic components (Tomimura & Eriguchi 2005; Yoshida & Eriguchi 2006; Yoshida et al. 2006; Lander & Jones 2009; Otani et al. 2009) in a non-perturbative manner.

It should be noted that the twisted-torus magnetic configuration that appears during the evolutionary computations by Braithwaite & Spruit (2004) is qualitatively the same as one of the exact axisymmetric and stationary solutions obtained in Yoshida et al. (2006). Moreover, stable configurations of stellar magnetic fields must have a twisted-torus structure according to Braithwaite (2009). Concerning the stability analysis, this type of configurations is expected to be stable, while magnetic fields with purely *poloidal* configurations or purely *toroidal* configurations have been shown to be unstable (see e.g. Tayler 1973; Wright 1973; Markey & Tayler 1973; Flowers & Ruderman 1977).

In this paper, we apply the formulation developed by Tomimura & Eriguchi (2005), Yoshida & Eriguchi (2006) and Yoshida et al. (2006) in order to find out how strong and localized *poloidal* magnetic fields can exist inside stars, as far as equilibrium configurations are concerned. In this formulation, the electric current density consists of several terms with different physical significances which contain arbitrary functionals of the magnetic flux function. These arbitrary functions correspond to the degrees of freedom in magnetized equilibria. One of the arbitrary functionals in the expression for the electric current density corresponds to the current in the *toroidal* direction. By choosing this functional form properly, we would be able to obtain equilibrium configurations of axisymmetric barotropic stars with highly localized and extremely strong *poloidal* magnetic fields.

2 FORMULATION AND NUMERICAL METHOD

Since we employ the formulation developed by Tomimura & Eriguchi (2005), Yoshida & Eriguchi (2006), and Yoshida et al. (2006), here we summarize the main scheme briefly and explain newly introduced parts in detail.

2.1 Assumptions and basic equations

We make the following assumptions for the magnetized stars.

- (i) The system is in a stationary state, i.e. $\frac{\partial}{\partial t} = 0$.
- (ii) When stars are rotating and have magnetic fields, the rotational axis and the magnetic axis coincide.
- (iii) The rotation is rigid.
- (iv) The configurations are axisymmetric about the magnetic or the rotational axis, i.e. $\frac{\partial}{\partial \varphi} = 0$, where we use the spherical coordinates (r, θ, φ) .
- (v) The configurations are symmetric with respect to the equator.
- (vi) There are no meridional flows.
- (vii) The star is self-gravitating.
- (viii) The systems are treated in the framework of non-relativistic physics.
- (ix) The conductivity of the stellar matter is infinite, i.e. the ideal magnetohydrodynamics (MHD) approximation is employed.

(x) No electric current is assumed in the vacuum region.

(xi) The barotropic equation of state is assumed :

$$p = p(\rho) . \quad (1)$$

Here p and ρ are the pressure and the mass density, respectively. Assumptions of axisymmetric and equatorial symmetries as well as rigid rotation are adopted here in order to simplify our investigations.

In a rotating star under a radiative equilibrium, there appears to be meridional flow in special cases. However, we neglect it because the time scale is many orders of magnitude larger than the (magneto)hydrodynamic one (Tassoul 2000). Also, there is a suggestion that gradual diffusion of the internal magnetic fields drives a meridional flow (Urpin & Ray 1994). The time scale of this, again, is much larger than the (magneto)hydrodynamic one. Thus it is also neglected.

Under these assumptions, the basic equations are written as follows. The continuity equation is expressed as

$$\nabla \cdot (\rho \mathbf{v}) = 0 , \quad (2)$$

where \mathbf{v} is the fluid velocity. The equations of motion in the stationary state are written as:

$$\frac{1}{\rho} \nabla p = -\nabla \phi_g + R\Omega^2 \mathbf{e}_R + \frac{1}{\rho} \left(\frac{\mathbf{j}}{c} \times \mathbf{H} \right) , \quad (3)$$

where ϕ_g , Ω , \mathbf{j} , c and \mathbf{H} are gravitational potential, angular velocity, electric current density, speed of light and magnetic field, respectively. Here we use the cylindrical coordinates (R, φ, z) and \mathbf{e}_R is the unit vector in the R -direction. The gravitational potential satisfies Poisson equation:

$$\Delta \phi_g = 4\pi G \rho , \quad (4)$$

where G is the gravitational constant. Maxwell's equations are written as,

$$\nabla \cdot \mathbf{E} = 4\pi \rho_e , \quad (5)$$

$$\nabla \cdot \mathbf{H} = 0 , \quad (6)$$

$$\nabla \times \mathbf{E} = 0 , \quad (7)$$

$$\nabla \times \mathbf{H} = 4\pi \frac{\mathbf{j}}{c} , \quad (8)$$

where ρ_e and \mathbf{E} are the electric charge density and the electric field, respectively. Notice that we neglect the displacement current term in Eq.(7) as is common in MHD approximation. The ideal MHD condition, or the generalized Ohm's equation, can be expressed as:

$$\mathbf{E} = -\frac{\mathbf{v}}{c} \times \mathbf{H} . \quad (9)$$

We choose two kinds of barotropic equations of state. One is the polytropic equation of state:

$$p = K_0 \rho^{1+1/N} , \quad (10)$$

where N and K_0 are the polytropic index and the polytropic constant, respectively. The other is the degenerated Fermi gas at zero temperature, defined as

$$p = a[x(2x^2 - 3)\sqrt{x^2 + 1} + 3 \ln(x + \sqrt{x^2 + 1})] , \quad (11)$$

where

$$\rho = bx , \quad (12)$$

$$a = 6.00 \times 10^{22} \text{ dyn/cm}^2, \quad (13)$$

$$b = 9.825 \times 10^5 \mu_e \text{ g/cm}^3. \quad (14)$$

Here μ_e is the mean molecular weight. We fix $\mu_e = 2$ in all our computations here, which corresponds to a fully ionized pure hydrogen gas. This choice of parameters is same as that in Hachisu (1986).

2.2 The form of the current density and the boundary condition

From the assumptions of axisymmetry and stationarity, we introduce magnetic flux function Ψ as follows:

$$H_R \equiv -\frac{1}{R} \frac{\partial \Psi}{\partial z}, \quad H_z \equiv \frac{1}{R} \frac{\partial \Psi}{\partial R}, \quad (15)$$

where H_R and H_z are magnetic field components in the R -direction and z -direction, respectively. We assume this flux function is positive in the entire space. By introducing this magnetic flux function, equation (6) can be automatically satisfied. It should be noted that the magnetic flux function Ψ can be expressed as:

$$\Psi = r \sin \theta A_\varphi, \quad (16)$$

where A_φ is the φ -component of the vector potential $\mathbf{A} = (A_R, A_\varphi, A_z)$.

As shown in Tomimura & Eriguchi (2005), for axisymmetric and stationary barotropes with rigid rotation we can constrain the form of the electric current density by using an integrability condition of the equations of motion, equation (3):

$$\frac{\mathbf{j}}{c} = \frac{1}{4\pi} \frac{d\kappa(\Psi)}{d\Psi} \mathbf{H} + r \sin \theta \rho \mu(\Psi) \mathbf{e}_\varphi, \quad (17)$$

where $\kappa(\Psi)$ and $\mu(\Psi)$ are arbitrary functions of the magnetic flux function Ψ . Notice, in particular, that the *toroidal* component of magnetic field is given as

$$H_\varphi = \frac{\kappa(\Psi)}{r \sin \theta} \quad (18)$$

which can be derived from equations (3), (8) and (17). It should be noted that these two arbitrary functions are conserved along the *poloidal* magnetic field lines. Although the meanings of these two functions are described in previous works (see, e.g., Lovelace et al. 1986), in this paper we will explain their meanings differently from our point of view.

Since we have assumed that there is no electric current in the vacuum region, in other words that there is no *toroidal* magnetic field outside the star (see equation 17), the form for κ needs to be a special one. The simplest form can be $\kappa = \text{constant}$ (Ioka & Sasaki 2004, Haskell et al. 2008), but for this choice of κ the *toroidal* magnetic field would extend to the vacuum region. In order to avoid this possibility, we choose the functional form of κ as follows:

$$\kappa(\Psi) = \begin{cases} 0, & \text{for } \Psi \leq \Psi_{\max}, \\ \frac{\kappa_0}{k+1} (\Psi - \Psi_{\max})^{k+1}, & \text{for } \Psi \geq \Psi_{\max}, \end{cases} \quad (19)$$

This choice of κ is the same as that in Yoshida & Eriguchi (2006) and Lander & Jones (2009). In this paper we fix $k = 0.1$. Equations (18) and (19) ensure that the *toroidal* magnetic

field vanishes smoothly at the stellar surface. Incidentally, using these functionals, we obtain the first integral of equation (3) as follows:

$$\int \frac{dp}{\rho} = -\phi_g + \frac{1}{2} (r \sin \theta)^2 \Omega_0^2 + \int \mu(\Psi) d\Psi + C, \quad (20)$$

where C is an integration constant. The first term of the right-hand side is the gravitational potential. The second term on the right hand side is related to rotation. We can consider it as a rotational potential. Similarly, the third term means the potential of Lorentz force. We can regard this term as the magnetic force potential. Therefore, $\int \mu d\Psi$ is considered to be non-force-free contribution from the current density, as is seen in equation (17). Since the Lorentz force is given by the cross product $\mathbf{j}/c \times \mathbf{H}$, the first term of equation (17) has no effect on the equation of motion, i.e. it is force-free, and only the second term contributes to the Lorentz force, i.e., non force-free. The distribution of Lorentz force could be changed by adopting different functional forms for μ . All previous works (Tomimura & Eriguchi 2005, Yoshida & Eriguchi 2006, Yoshida et al. 2006, Lander & Jones 2009, Otani et al. 2009) fixed $\mu = \mu_0$ (constant). We choose a different functional form for μ in this paper as follows:

$$\mu(\Psi) = \mu_0 (\Psi + \epsilon)^m, \quad (21)$$

$$\int \mu(\Psi) d\Psi = \frac{\mu_0}{m+1} (\Psi + \epsilon)^{m+1}, \quad (22)$$

where m and ϵ are two constant parameters. In order to avoid singular behavior, we fix $\epsilon = 1.0 \times 10^{-6}$ in all calculations. As we shall see below, the parameter m determines a degree of localization of the interior *poloidal* magnetic field. We assume that *poloidal* magnetic fields extend throughout the whole space and that there are no discontinuities even at the stellar surface. The global magnetic field configurations of our models are nearly dipole-like because of the requirement of the functional form for κ at the stellar surface. These configurations contain closed *poloidal* magnetic field lines inside the star. The flux function Ψ attains its maximum at the central parts of these closed field lines and it takes its minimum on the symmetric axis and at infinity. The minimum value is zero because of $\Psi = r \sin \theta A_\varphi$ and the boundary condition for $A_\varphi = 0$ at infinity. The magnetic potential ($\int \mu d\Psi$) changes its qualitative behavior in its spatial distribution when $m = -1$. If we adopt $m < -1$, as Ψ decreases from its maximum to zero on the axis of the star the value of the magnetic potential increases unboundedly if $\epsilon \rightarrow 0$. As a result, the *poloidal* magnetic field lines are concentrated near the axis in order to fulfill such magnetic potential distributions. On the other hand, if we choose $m > -1$, the value of the magnetic potential decreases as Ψ decreases from its maximum to zero, which is realized on the axis. Then the *poloidal* magnetic field lines are distributed more uniformly than those for configurations with $m < -1$. If we choose $m = 0$, we obtain $\mu = \text{constant}$ configurations. They are the same as those investigated by other authors.

It is remarkable that the only freedom that we can take in our formulation is related to the choices of functional forms and the values of the parameters which appear in those functions. It implies that degrees of freedom for choices for these functions and parameters correspond to degrees of freedom for many kinds of stationary axisymmetric magnetic field con-

figurations. In fact, as we see from our results, different values for m result in qualitatively different distributions for the magnetic potentials and the *poloidal* magnetic fields. In other words, we can control the magnetic field distributions to a certain extent by adjusting the value for m . This is the reason why we use this functional form of μ in this paper.

After we choose the functional form of the current density, by using Eq.(17) and the definition of the vector potential, we obtain the following partial differential equation of the elliptic type:

$$\Delta(A_\varphi \sin \varphi) = 4\pi S_A(r, \theta) \sin \varphi, \quad S_A \equiv -\frac{j_\varphi}{c}. \quad (23)$$

As we have seen in the previous paragraph, all the physical quantities related to the vector potential can be expressed solely by Ψ . Therefore we need not solve for A_R and A_z . It implies that our present formulation does not depend on the gauge condition for the vector potential \mathbf{A} . Next we impose the boundary conditions for the gravitational potential and the vector potential, chosen as follows:

$$\phi_g \sim \mathcal{O}\left(\frac{1}{r}\right), \quad (r \rightarrow \infty), \quad (24)$$

$$A_\varphi \sim \mathcal{O}\left(\frac{1}{r}\right), \quad (r \rightarrow \infty). \quad (25)$$

This boundary condition for A_φ results in

$$H_p \sim \mathcal{O}\left(\frac{1}{r^2}\right), \quad (r \rightarrow \infty). \quad (26)$$

where H_p is the *poloidal* magnetic field. From these boundary conditions and using a proper Green's function for the Laplacian, we have the integral representations of equation (4) and equation (23) as follows:

$$\phi_g(\mathbf{r}) = -G \int \frac{\rho(\mathbf{r}')}{|\mathbf{r} - \mathbf{r}'|} d^3 \mathbf{r}', \quad (27)$$

$$A_\varphi(\mathbf{r}) \sin \varphi = - \int \frac{S_A(\mathbf{r}') \sin \varphi'}{|\mathbf{r} - \mathbf{r}'|} d^3 \mathbf{r}'. \quad (28)$$

Therefore, we can obtain smooth potentials, ϕ_g and A_φ by integrating these equations. Since we have chosen the functional form of the current density which decreases near the surface and vanishes at the stellar surface sufficiently smoothly, we obtain continuous *poloidal* magnetic fields from A_φ .

2.3 Global characteristics of equilibria

To see the global characteristic of magnetized equilibria, we define some integrated quantities as follows:

$$W \equiv \frac{1}{2} \int \phi_g \rho d^3 \mathbf{r}, \quad (29)$$

$$T \equiv \frac{1}{2} \int \rho (R\Omega)^2 d^3 \mathbf{r}, \quad (30)$$

$$\Pi \equiv \int p d^3 \mathbf{r}, \quad (31)$$

$$U \equiv N\Pi, \quad (32)$$

for polytropic models and

$$U \equiv \int g(x) d^3 \mathbf{r}, \quad (33)$$

$$g(x) = a\{8x^3[(x^2 + 1)^{\frac{1}{2}} - 1]\} - p, \quad (34)$$

for the Fermi gas configurations (see. Chandrasekhar 1939),

$$\mathcal{H} \equiv \int \mathbf{r} \cdot \left(\frac{\mathbf{j}}{c} \times \mathbf{H}\right) d^3 \mathbf{r}. \quad (35)$$

$$K \equiv \int (\nabla \times \mathbf{A}) \cdot \mathbf{A} d^3 \mathbf{r} = \int \mathbf{H} \cdot \mathbf{A} d^3 \mathbf{r}, \quad (36)$$

where W , T , Π , U , \mathcal{H} and K are the gravitational energy, rotational energy, total pressure, internal energy, magnetic field energy and magnetic helicity, respectively. In order to evaluate the structures of magnetic fields, we define some physical quantities related to the magnetic fields as follows:

$$H_{sur} = \frac{\int_0^{2\pi} \int_0^\pi r_s^2(\theta) \sin \theta |\mathbf{H}(r_s, \theta)| d\theta d\varphi}{S}, \quad (37)$$

where $r_s(\theta)$ and $|H_{sur}|$ are the stellar radius in the direction of θ and the surface magnetic field strength, respectively, and the surface area of the star is defined as:

$$S = \int_0^{2\pi} \int_0^\pi r_s^2(\theta) \sin \theta d\theta d\varphi. \quad (38)$$

The volume-averaged magnetic field strength in the central region of the star is defined as

$$H_c = \frac{\int_0^{2\pi} \int_0^\pi \int_0^{r_c} r^2 \sin \theta |\mathbf{H}(r, \theta)| dr d\theta d\varphi}{V}, \quad (39)$$

where we choose $r_c = 0.01r_e$ and V is the volume of the central region with $r \leq r_c$, defined as

$$V = \int_0^{2\pi} \int_0^\pi \int_0^{r_c} r^2 \sin \theta dr d\theta d\varphi. \quad (40)$$

This central region seems to be very small, but we can resolve it sufficiently because we use non-uniform and centrally concentrated meshes (see. Fig. A1 and Eq. A21 in Appendix). We have 77 meshes to resolve the region in actual numerical computations.

In order to know the contributions of the *poloidal* magnetic field and the *toroidal* magnetic field separately, we define the *poloidal* magnetic energy \mathcal{H}_p and the *toroidal* magnetic energy \mathcal{H}_t as

$$\mathcal{H}_p = \frac{1}{8\pi} \int_0^{2\pi} \int_0^\pi \int_0^\infty r^2 \sin \theta |H_r(r, \theta)^2 + H_\theta(r, \theta)^2| dr d\theta d\varphi, \quad (41)$$

$$\mathcal{H}_t = \frac{1}{8\pi} \int_0^{2\pi} \int_0^\pi \int_0^\infty r^2 \sin \theta |H_\varphi(r, \theta)^2| dr d\theta d\varphi, \quad (42)$$

As for the magnetic multipole moment seen outside a star, we compute each multipole component by solving the following equation in a vacuum:

$$\Delta(A_\varphi \sin \varphi) = 0. \quad (43)$$

Considering the boundary conditions at infinity and the symmetry of the magnetized stars, the solution of the above equa-

tion can be expressed as

$$A_\varphi \sin \varphi \equiv \sum_{n=1}^{\infty} A_{\varphi,n} \sin \varphi = \sum_{n=1}^{\infty} b_{n,1} r^{-n-1} Y_{n,1}(\theta, \varphi), \quad (44)$$

where $Y_{n,1}(\theta, \varphi)$ is the spherical harmonics of degree n and order $m = 1$. The coefficients $b_{n,1}$ correspond to the magnetic multipoles.

2.4 Setting for Numerical Computations

For numerical computations, the physical quantities are transformed into dimensionless ones using the maximum density ρ_{\max} , the maximum pressure p_{\max} and the equatorial radius r_e as follows:

$$\hat{r} \equiv \frac{r}{r_e} = \frac{r}{\sqrt{\frac{1}{\alpha} \frac{p_{\max}}{4\pi G \rho_{\max}^2}}}, \quad (45)$$

for polytropic configurations and

$$\hat{r} \equiv \frac{r}{r_e} = \frac{r}{\sqrt{\frac{1}{\alpha} \frac{8a}{b} \frac{1}{4\pi G \rho_{\max}^2}}}, \quad (46)$$

for the Fermi gas models, and

$$\hat{\rho} \equiv \frac{\rho}{\rho_{\max}}. \quad (47)$$

Here α is introduced so as to make the distance from the center to the equatorial surface of the star to be unity. Arbitrary functions are also transformed into dimensionless ones. Quantities with $\hat{\cdot}$ are dimensionless. For example, the dimensionless length is \hat{r} and the dimensionless arbitrary functions are $\hat{\mu}$ and $\hat{\kappa}$, respectively. Dimensionless forms of other quantities are collected in Appendix A1.

The computational domain is defined as $0 \leq \theta \leq \frac{\pi}{2}$ in the angular direction and $0 \leq \hat{r} \leq 2$ in the radial direction. Since the equation of magnetohydrostationary equilibrium is defined only inside the star and the source terms of the elliptic equations for the gravitational potential and the magnetic flux function vanish outside the star, our computational domain covers a region of the space that is sufficient for obtaining equilibria. In order to resolve the region near the axis sufficiently, we use a special coordinate in actual numerical computations. Total mesh numbers in r -direction and in θ -direction are 1025 and 1025, respectively. We describe details of the computational grid points in Appendix A2.

2.5 Numerical method

We use the scheme of Tomimura & Eriguchi (2005). This scheme is based on the Hachisu Self-Consistent Field (HSCF) scheme (Hachisu 1986), which is the method for obtaining equilibrium configurations of rotating stars. We define the ratio of the equatorial radius to the polar radius as the axis ratio q . This quantity q characterizes how distorted the stars are due to non-spherical forces. The stronger the non-spherical force becomes, the more distorted the stellar shape is. The non-spherical force can be the centrifugal force, the magnetic force or both of them. We fix the value of q in order to obtain the magnetized equilibria. We also fix one of $\hat{\mu}_0$ and $\hat{\Omega}_0$. If we fix $\hat{\mu}_0$, we will obtain the value of $\hat{\Omega}_0$ after the relaxation and

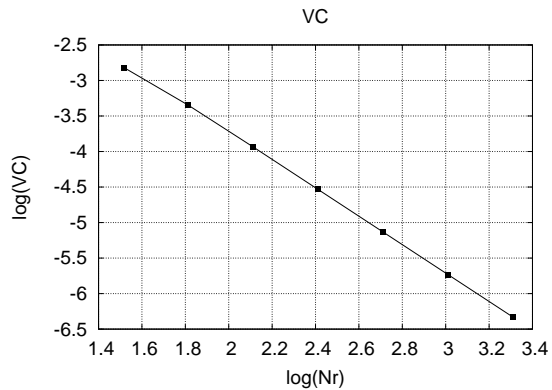


Figure 1. The virial quantity VC, plotted against the number of grid points in the r -direction.

iteration. If we fix $\hat{\Omega}_0$, we will obtain $\hat{\mu}_0$. Then, we will obtain one magnetized equilibrium state.

2.6 Numerical accuracy check

In order to check the accuracy of converged solutions, we compute a relative value of the virial relation as follows:

$$VC \equiv \frac{|2T + W + 3\Pi + \mathcal{H}|}{|W|}. \quad (48)$$

Since this quantity VC must vanish for exact equilibrium configurations, we can check the global accuracies of the numerically obtained models as a whole (see e.g. Hachisu 1986). Since the numerical results depend on mesh size, we have computed the same model by changing the number of grid points in the r -coordinate but fixing the number of grid points in the θ -direction as $n_\theta = 513$. Fig. 1 shows VC as a function of the number of grid points in the r -coordinate for polytropic models. Since we use schemes of second-order accuracy, VC decreases as the square inverse of the number of grid points (see also Lander & Jones 2009; Otani et al. 2009).

3 NUMERICAL RESULTS

We give a brief summary of our numerical results here. First we show the basic features for negative m models and the dependences of the magnetic field configurations on the values of m for barotropes. We also show rotating and magnetized polytropic models in order to examine the effect of rotation on magnetic fields. The influence of the equation of state on the interior magnetic field is also displayed. We have computed $N = 0.5, 1, 1.5$ polytropic models and four white dwarf models with $\rho_c = 1.0 \times 10^7, 1.0 \times 10^8, 1.0 \times 10^9$, and $1.0 \times 10^{10} \text{ g cm}^{-3}$.

3.1 Effect of the distribution of the toroidal current density on the distribution of the magnetic field

We show the results for the distributions of the magnetic fields for different values of m . In particular, in order to examine the effect of magnetic fields alone, we consider configurations

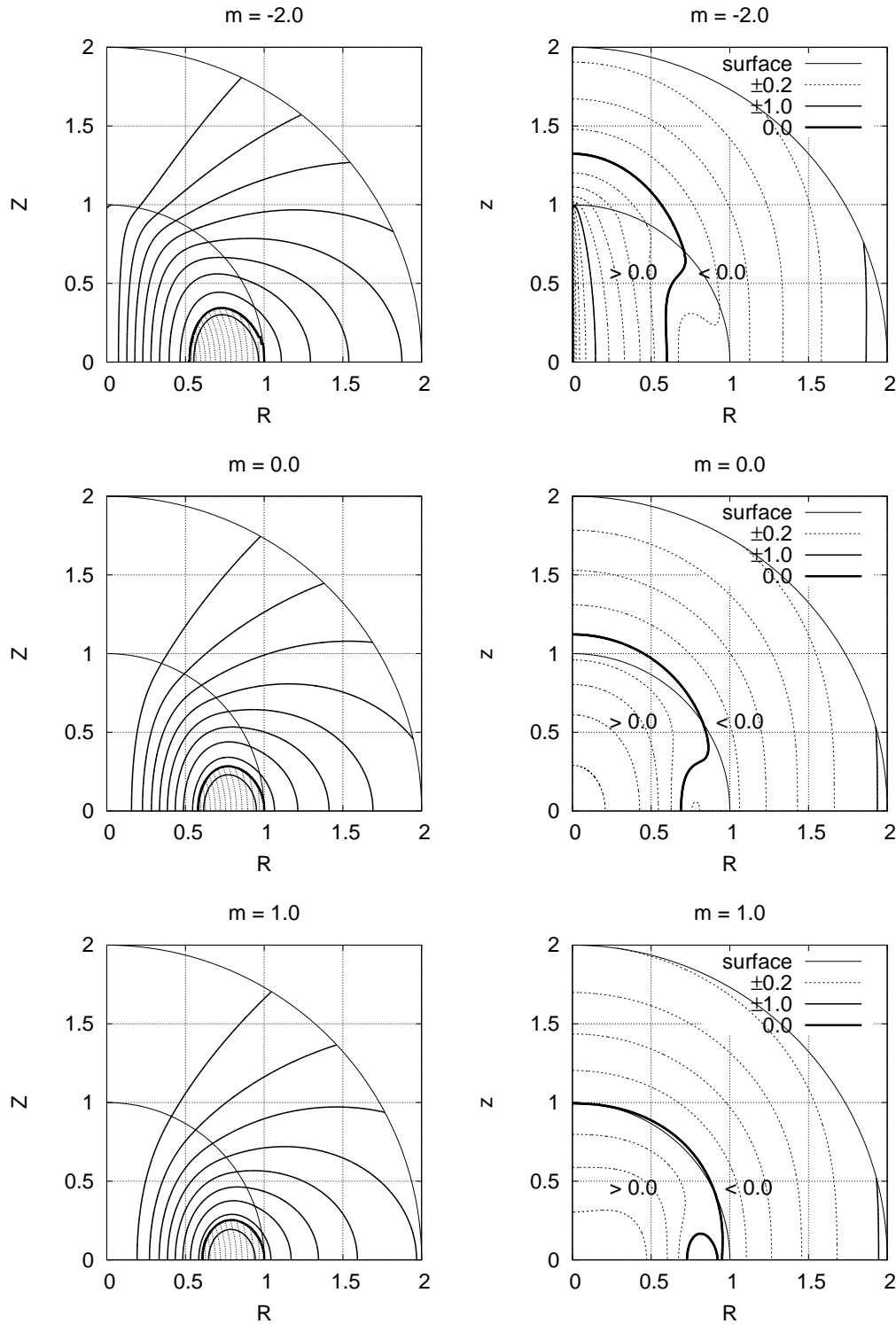


Figure 2. Contours for the magnetic flux function (left panels) and for the logarithm of the strength of the magnetic field normalized by the averaged surface magnetic field (right panels) are shown. The inner solid circle corresponds to the surface of the star and the outer solid circle denotes the boundary of our computational region. The flux difference between two adjacent contours of thick lines is $1/10$ of the maximum value of Ψ . In the left panels, the thick *poloidal* field line is the boundary of the *toroidal* magnetic field region. The *toroidal* magnetic field exists only inside the region. In the right panels, the distribution of the logarithm of the magnetic field normalized by the averaged surface magnetic field, $\log_{10} |\mathbf{H}/H_{sur}|$ contour, is shown. The thick solid curve corresponds to the curve with $\log_{10} |\mathbf{H}/H_{sur}| = 0$. Inside this curve $\log_{10} |\mathbf{H}/H_{sur}| > 0$ and outside this curve $\log_{10} |\mathbf{H}/H_{sur}| < 0$. The difference between two adjacent contours is 0.2.

m	$1 - q$	H_c/H_{sur}	$\mathcal{H}_p/\mathcal{H}$	$\mathcal{H}/ W $	$\Pi/ W $	α	$\hat{\mu}_0$	\hat{K}	VC
$N = 1.0$									
-2.0	2.2E-2	1.03E+2	9.987E-1	3.74E-5	3.33E-1	5.07E-2	2.28E-9	7.76E-7	5.132E-8
-1.5	1.9E-3	4.44E+1	9.982E-1	3.02E-5	3.33E-1	5.07E-2	9.65E-8	8.27E-7	2.646E-6
-1.1	4.2E-4	2.19E+1	9.978E-1	2.60E-5	3.33E-1	5.07E-2	1.80E-6	8.33E-7	2.775E-6
-0.9	2.5E-4	1.62E+1	9.976E-1	2.45E-5	3.33E-1	5.07E-2	7.74E-6	8.35E-7	2.785E-6
-0.5	1.3E-4	1.02E+1	9.972E-1	2.21E-5	3.33E-1	5.07E-2	1.41E-4	8.35E-7	2.788E-6
0.0	8.8E-5	7.17E+0	9.968E-1	1.99E-5	3.33E-1	5.07E-2	5.25E-3	8.31E-7	2.789E-6
0.5	7.0E-5	5.69E+0	9.963E-1	1.83E-5	3.33E-1	5.07E-2	1.92E-1	8.23E-7	2.789E-6
1.0	6.1E-5	4.78E+0	9.959E-1	1.70E-5	3.33E-1	5.07E-2	6.90E+0	8.11E-7	2.789E-6

Table 1. Physical quantities for $\hat{\Omega}_0 = 0$, $\hat{\kappa}_0 = 10$ and $H_{sur} = 1.5 \times 10^{15}$ G polytropes with different values of m .

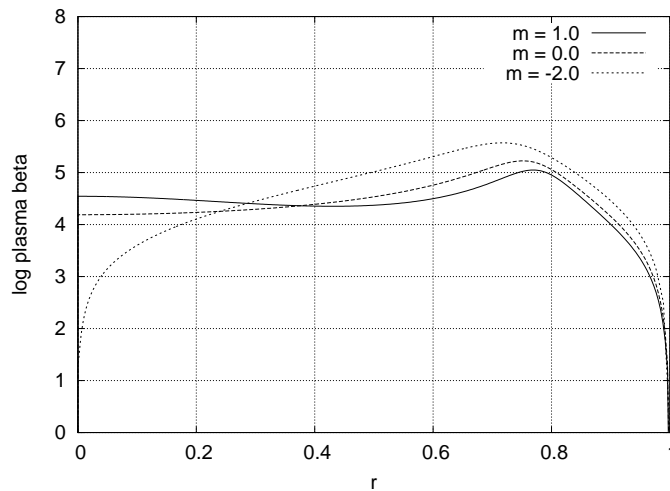


Figure 3. Profiles of $\log \beta$ at $\theta = \pi/2$, where β is the plasma β . Solid line represents the distribution for an $m = 1.0$ configuration, dashed line that for an $m = 0.0$ configuration and dotted line that for an $m = -2.0$ model, respectively.

without rotation. The effect of stellar rotation is discussed in Sec. 3.2. Thus we set $\hat{\Omega}_0 = 0$ and compute $N = 1$ polytropic equilibrium models with different values of m and appropriate values of q so that the surface magnetic field becomes roughly $H_{sur} = 10^{15}$ G when $\rho_c = 1.0 \times 10^{15} \text{ g cm}^{-3}$ and mass $M = 1.4M_\odot$. By setting $N = 1$ and an appropriate choice of polytropic constant K of $p = K\rho^2$, we obtain models with $M = 1.4M_\odot$. It should be noted that these models have the typical mass and radius for neutron stars. We choose $N = 1$ as a simple approximation of neutron stars here. We searched and found the value of q by calculating many equilibrium states.

Physical quantities of these models are shown in Table 1. It can be seen that values of $\Pi/|W|$ and α are almost the same among these models. Although the strength of the averaged surface magnetic field is $H_{sur} = 1.5 \times 10^{15}$ G, the values of $\mathcal{H}/|W|$ are much smaller than those of $\Pi/|W|$. It implies that the effect of the magnetic fields in these configurations on their global structures is very small. On the other hand, values of H_c/H_{sur} and $\mathcal{H}/|W|$ vary rather considerably for different values of m . As the value of m is decreased, values of H_c/H_{sur} and $\mathcal{H}/|W|$ increase. In Fig. 2 the structure and strength of magnetic fields are shown for three different values of m , i.e. $m = -2.0$ (negative m model), $m = 0.0$ ($\hat{\mu} = \text{constant}$ model) and $m = 1.0$ (positive m model). The left-hand

panels show the *poloidal* magnetic field lines and the regions where the *toroidal* magnetic field exists. The right-hand panels display the strength of the magnetic field $|\mathbf{H}|$ normalized by the averaged surface magnetic field H_{sur} .

As seen from these figures, there are no discontinuities of the magnetic fields at the stellar surfaces. Due to the choice of the functional form of the arbitrary function $\hat{\kappa}(\hat{\Psi})$ and the distribution of the magnetic flux function, *toroidal* magnetic fields appear only in the region that is bounded by the outermost closed *poloidal* magnetic field line inside the star (thick line). Thus the toroidal magnetic fields exist inside the torus region.

As the value of m is increased, i.e. from top panels to bottom panels, the ratio of H_c/H_{sur} decreases (see left panels in Fig. 2) because the *poloidal* magnetic field becomes weaker. This is also related to the fact that the interior *poloidal* magnetic field lines are much more localized near the axis for negative m models. The contours of magnetic field strength also display the same tendency. For the $m = 1.0$ model, the contour of $|\mathbf{H}| = H_{sur}$ (thick line) shows the stellar surface and the shapes of contours are nearly spherical. By contrast, the contours of the $m = -2.0$ model are highly distorted near the axis. The strength of the *poloidal* magnetic fields for the negative m models could exceed 10^{17} G near the central re-

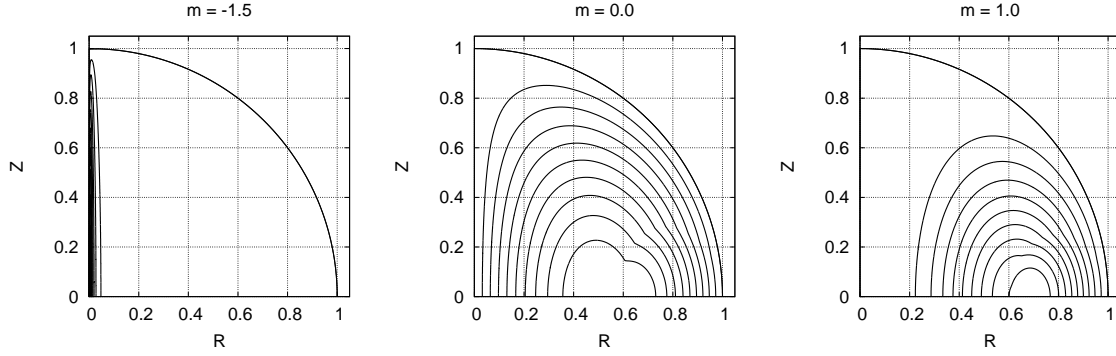


Figure 4. Isocontours of j_φ for different values of m . These panels show $N = 1$, $q = 0.99$ polytropic equilibrium models. The outermost curve denotes the stellar surface. The difference between two adjacent contours is $1/10$ times the maximum of j_φ . The current is non-zero in the whole star except at the stellar surface and the symmetric axis (z -axis).

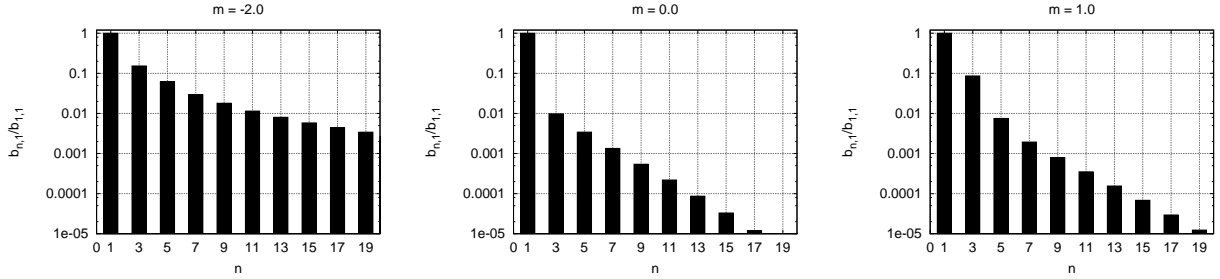


Figure 5. The ratio of the magnetic 2^n -pole moment coefficient to the magnetic dipole moment coefficient, $|b_{n,1}/b_{1,1}|$, is plotted against the multipole moment number n . Here $b_{n,1}$ is defined in Eq. (44).

gion. Fig. 3 shows the profiles of the plasma β on the $\theta = \pi/2$ plane, i.e. on the equatorial plane. Here, the plasma β is defined as follows:

$$\beta = 8\pi p / |\mathbf{H}|^2. \quad (49)$$

This quantity denotes the contribution of the gas pressure effect compared with the magnetic pressure effect. Fig. 3 shows profiles of β for models with $m = -2.0, 0.0, 1.0$. As seen from Fig.3, the profiles of β are very similar to each other near the stellar surface regions. For the region around $\hat{r} \sim 0.6$, however, the value of β for the $m = -2.0$ model is larger than those for the $m = 0$ and $m = 1.0$ models. Since these models have almost the same mass density distributions, this difference means a difference of magnetic pressure distribution. In this region the magnetic field of the $m = -2.0$ configuration is weaker and thus the β becomes larger. However, *it should be noted that* these contours for the model with $m = -2.0$ are rather confined to the very narrow region near the central part. In other words, the gradient of the magnetic field distribution for the model with $m = -2$ is much steeper than the gradient of the gas pressure distribution compared with the models with $m = 1.0$ and $m = 0.0$. Thus the value of $\log \beta$ becomes dramatically small within the $\hat{r}[0 : 0.1]$ region and the minimum value of β can reach about ~ 20 in the central part. Therefore, in the central region of the model with $m = -2.0$ the influence of magnetic field on the local structure of the star is no longer negligible.

Here we explain the reason why this kind of highly lo-

calized *poloidal* magnetic field configuration can be realized. We need to note the distribution of the *toroidal* current density \hat{j}_φ in order to analyse our models properly, because the current density is related to the magnetic field closely by the two equations (8) and (17). In Fig. 4 we show the distributions of the *toroidal* current density for models with different values of m . As seen from Fig. 4, the distribution of the *toroidal* current density is concentrated toward the magnetic axis for the configuration with negative values of m . This is due to the dependence of $\hat{\mu}$ on the value of m . The current density distribution spreads over a large region inside the star as the value of m increases (from left panel to right panel). In other words, the distribution of the magnetic flux function becomes more and more concentrated toward the magnetic axis as the value of m decreases. It implies that the strengths of magnetic fields for models with negative values of m become very great near the magnetic axis. Our results show one possibility that a strong *poloidal* magnetic field can exist deep inside a star. If such a strong *poloidal* magnetic field is sustained deep inside a star, the contours of the magnetic field strength are no longer nearly spherical as in the bottom right panel of Fig. 2. Although this feature might be modified by dropping the assumption of the axisymmetry, it would give us one possibility for the presence of a strong *poloidal* magnetic field configuration deep inside a star.

Finally, to characterize the magnetic structure we show the magnetic multipole moments of magnetized stars. In Fig. 5 the values of $|b_{n,1}/b_{1,1}|$ (equation 44) are plotted. There ap-

pear to be only multipolar magnetic moments with odd degree ($n = 1, 3, 5$), because we have assumed the equatorial symmetry. As seen from these figures, in configurations with negative values of m the higher order magnetic multipole moments contribute ($|b_{n,1}/b_{1,1}|$) significantly to the total magnetic field, while in configurations with positive values of m the magnetic dipole moment is the dominant component of the total magnetic field. These figures show that the external magnetic field is nearly dipole when we adopt $m = 0$ but it is not simple dipole when $m > 0$ and $m < 0$. From the left panel, we see that the $n = 3$ (octupole) component reaches about a few tens of per cent of the dipole component when $m = -2.0$.

3.2 Effect of stellar rotation

We calculate two sequences with rotation for different values of m in order to examine the influence of rotation. We choose the value of $\hat{\mu}_0$ by obtaining a configuration with $\hat{\Omega}_0 = 0$ and $q = 0.99$ as a non-rotating limit of our equilibrium sequence. We choose $q = 0.99$ here for simplicity. The value of $q = 0.99$ corresponds to an equilibrium configuration with $H_{sur} \sim 10^{15}$ G when we consider a typical neutron star model with negative m . We have obtained sequences of stationary configurations by fixing the parameters m and $\hat{\mu}_0$ and changing the value of q . By changing the value of q for a fixed value of $\hat{\mu}_0$, we have equilibrium configurations with shapes that are deformed from spheres by rotational effect in addition to the magnetic force. Since we fix the magnetic potential parameter $\hat{\mu}_0$ and m along one sequence, the equilibrium sequence is the one with approximately constant magnetic effect. If the values of m and $\hat{\mu}_0$ are changed, we will be able to solve another stationary sequence. We have calculated two stationary sequences with negative m ($m = -1.5$) and with $m = 0.0$, i.e. $\hat{\mu} = \text{constant}$.

Physical quantities of stationary configurations are tabulated in Table 2. As seen from this table, the quantities $|\hat{W}|$ and α or the ratio $\Pi/|W|$ and $T/|W|$ depend on the strength of the rotation. By contrast, magnetic quantities are almost unaffected by rotation. The dependence of the ratio H_c/H_{sur} on rotation is relatively small. The equilibrium configurations with highly localized magnetic fields that we have obtained in this paper are almost unchanged even by rapid rotation. Therefore, we do not consider the effect of rotation any longer in this paper.

3.3 Effect of equations of state

Thus far, we have discussed our magnetized configurations by showing the results for $N = 1$ polytropic models. The distribution of the *toroidal* current density, however, depends on the mass density profile through equation (17). Thus we show other polytropic models, i.e. $N = 0.5$ and $N = 1.5$ polytropes, as well as configurations for degenerate gases, i.e. white dwarf models, in order to examine the influence of equations of state on configurations with highly localized magnetic fields.

We set $q = 0.99$ for polytropes and $q = 0.999$ for degenerate gases. The degenerate model with $q = 0.999$ corresponds to a configuration with a $H_{sur} \sim 1.0 \times 10^9$ G

magnetized white dwarf with $m = -3.0$, the central density is $1.0 \times 10^8 \text{ gcm}^{-3}$. This central density results in a white dwarf of about $1.16M_\odot$. Neither models rotates. We calculate 11 models with fixed values for q by setting $m = -3.0, -2.5, -2.0, -1.5, -1.1, -0.9, -0.5, 0.0, 0.5, 1.0, 1, 3$ and examine the dependence of H_c/H_{sur} on the equation of state.

Fig. 6 displays the ratio H_c/H_{sur} against the value of m for different equations of state. The dependency of this ratio on the value of m is qualitatively similar for these equations of state. Whichever equation of state we choose, we obtain configurations with highly localized magnetic fields, for which H_c/H_{sur} can exceed 100. The same is true for white dwarfs with highly localized magnetic fields. However, H_c/H_{sur} tends to become smaller for stiffer equations of state, as seen from Fig. 6.

Fig. 7 and Fig. 8 display the distribution of mass density, current density and the contour of $\log_{10} |\mathbf{H}|/H_{sur}$ of $m = -0.99$ configurations. Fig. 7 shows results for polytropes $N = 0.5$ and $N = 1.5$ (stiffest and softest equations of state among the polytropic models considered here) and Fig. 8 shows results for white dwarfs with $\rho_c = 1.0 \times 10^7 \text{ gcm}^{-3}$ and $\rho_c = 1.0 \times 10^{10} \text{ gcm}^{-3}$ (stiffest and softest among the white dwarf models considered here). As seen from top panels in each figure, the mass density distributions of the softer equation of state ($N = 1.5$ and $\rho_c = 1.0 \times 10^{10} \text{ gcm}^{-3}$) are more centrally concentrated than those of the stiffer equation of state ($N = 0.5$ and $\rho_c = 1.0 \times 10^7 \text{ gcm}^{-3}$). The current density distributions are also more centrally concentrated compared with the mass density distribution (middle panels). As a result, the *poloidal* magnetic fields become more highly localized for the softer equation of state (bottom panels). The mass of the white dwarf becomes higher for the higher central density. This implies that higher mass white dwarfs can have stronger interior magnetic fields deep inside if the magnetic field structure is fixed as in the present study.

4 DISCUSSION AND CONCLUSIONS

In this paper we have constructed axisymmetric and stationary magnetized barotropes that have extremely strong *poloidal* magnetic fields around the central region near the magnetic axis. The strength of the magnetic field in that region could be two orders of magnitude larger than that of the surface magnetic field. In the context of the neutron star physics, this would imply that there might be magnetars whose interior magnetic fields amounting to 10^{17} G if we assume the surface field to be order of 10^{15} G and that there might be magnetized white dwarfs with interior magnetic fields that reach 10^{12} G when the mass is nearly the Chandrasekhar limit and the surface field is of the order of 10^9 G.

Moreover, it should be noted that highly localized magnetized stars could have higher order magnetic multipole moments in addition to the dipole moment. Although in most astrophysical situations magnetic dipole fields have been assumed, we may need to consider configurations with contributions from higher multipole magnetic moments for some situations. In those cases, configurations with negative values of m might be used to analyze such systems.

q	H_c/H_{sur}	$\mathcal{H}_p/\mathcal{H}$	$ \hat{W} $	$\mathcal{H}/ W $	$\Pi/ W $	$T/ W $	α	$\hat{\Omega}_0^2$	\hat{K}	VC
			$m = -1.5$		$\hat{\mu}_0 = 5.070\text{E-}7$					
0.99	4.75E+1	0.9979	9.71E-2	1.14E-4	3.33E-1	0.00E+0	5.06E-2	0.00E+0	3.33E-6	1.80E-6
0.9	4.54E+1	0.9972	8.00E-2	1.26E-4	3.19E-1	2.14E-2	4.51E-2	1.17E-2	3.61E-6	3.41E-5
0.8	4.36E+1	0.9960	6.16E-2	1.45E-4	3.02E-1	4.67E-2	3.87E-2	2.36E-2	3.95E-6	1.34E-5
0.7	4.19E+1	0.9940	4.40E-2	1.74E-4	2.85E-1	7.30E-2	3.22E-2	3.37E-2	4.32E-6	5.70E-6
			$m = 0.0$		$\hat{\mu}_0 = 5.520\text{E-}2$					
0.99	6.98E+0	0.9947	9.60E-2	2.31E-3	3.33E-1	0.00E+0	5.03E-2	0.00E+0	1.20E-4	1.85E-6
0.9	6.63E+0	0.9934	7.90E-2	2.35E-3	3.18E-1	2.14E-2	4.48E-2	1.16E-2	1.15E-4	1.24E-6
0.8	6.29E+0	0.9913	6.05E-2	2.39E-3	3.01E-1	4.73E-2	3.83E-2	2.37E-2	1.06E-4	1.36E-6
0.7	5.99E+0	0.9878	4.32E-2	2.39E-3	2.83E-1	7.40E-2	3.18E-2	3.37E-2	9.24E-5	1.51E-6

Table 2. Physical quantities of two sequences with $m = 0.0$ and $m = -1.5$.

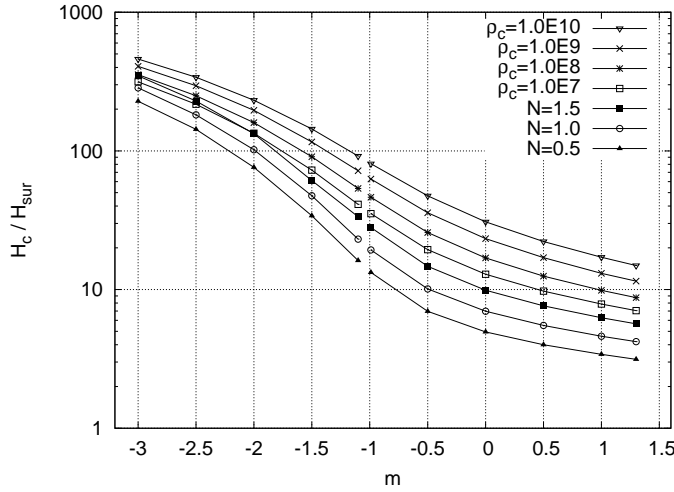


Figure 6. The value of H_c/H_{sur} is plotted against the value of m for polytropes ($q = 0.99$) and white dwarfs ($q = 0.999$).

4.1 Higher order magnetic multipole moments with even n

It should be noted that in the analysis of this paper only higher magnetic multipole moments with odd $n = 2\ell + 1$ where ℓ is an integer, i.e. $2^{2\ell+1}$ moments, appear and that there are no higher magnetic multipole moments with even $n = 2\ell$. This is due to the choice of the current density. Our choice of the arbitrary function $\mu(\Psi)$ and the assumption of the symmetry of Ψ about the equator necessarily result in magnetic field distributions that are symmetric about the equator. It implies that the magnetic field should penetrate the equator and that $2^{2\ell}$ type distributions that are confined the upper or lower half of the space of the equator are excluded. In order to obtain closed magnetic field distributions in the half plane above or below the equator, the current density must be chosen so as to flow in opposite directions above and below the equatorial plane. It also implies that we need to set the current density on the equator in the φ -direction to vanish.

Concerning $2^{2\ell}$ multipole magnetic moments distributions, Ciolfi et al. (2009) have obtained such configurations. Their solutions correspond to the choice of the current density distributions that are antisymmetric about the equator.

4.2 Forms of arbitrary functions

One might think it curious that functions appear in the formulation and that there is no physical principle specifying how to choose those arbitrary functional forms. The same situation appears for the problem of calculating equilibrium structures or stationary structures of rotating and axisymmetric *barotropes*. For that problem, the three component equations of the equations of motion do not remain independent but come to depend on each other. This implies that one could not solve for all the three components of the flow velocity completely. Assumptions of the *stationarity* and *barotropy* reduce the problem to a degenerate problem concerning the components of the flow velocity. Although there are *three* component equations for the *three* components of the flow velocity, those three component equations are no more independent. They become dependent each other due to the *barotropic nature* of the assumption for the gas. Therefore, one needs to *specify the rotation law or corresponding relation* in order to find stationary or equilibrium configurations for axisymmetric barotropes. The form of the rotation law is *arbitrary*.

The only requirement for the functional form regarding the rotation law comes from the nature of the stability of the system. However, one needs to know the stability of the system

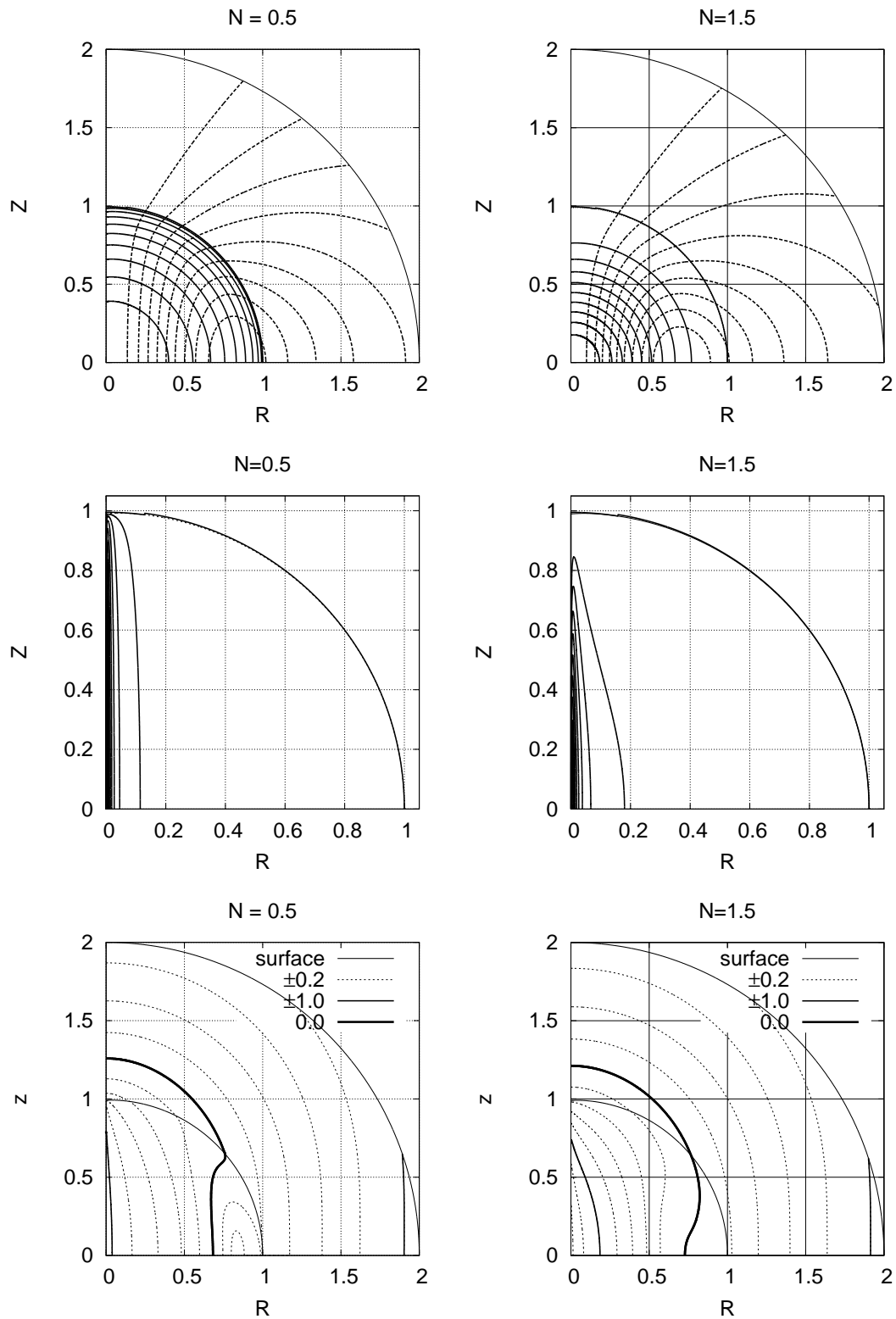


Figure 7. Isocontours for ρ and Ψ (top), j_φ (middle) and $\log[|\mathbf{H}|/|H_{sur}|]$ (bottom). These panels are for configurations with $m = -0.99$. The left panels are contours for the model of a $N = 0.5$ polytrope and the right panels are for a $N = 1.5$ polytrope. The difference between two adjacent contours is $1/10$ times the maximum of the corresponding quantities.

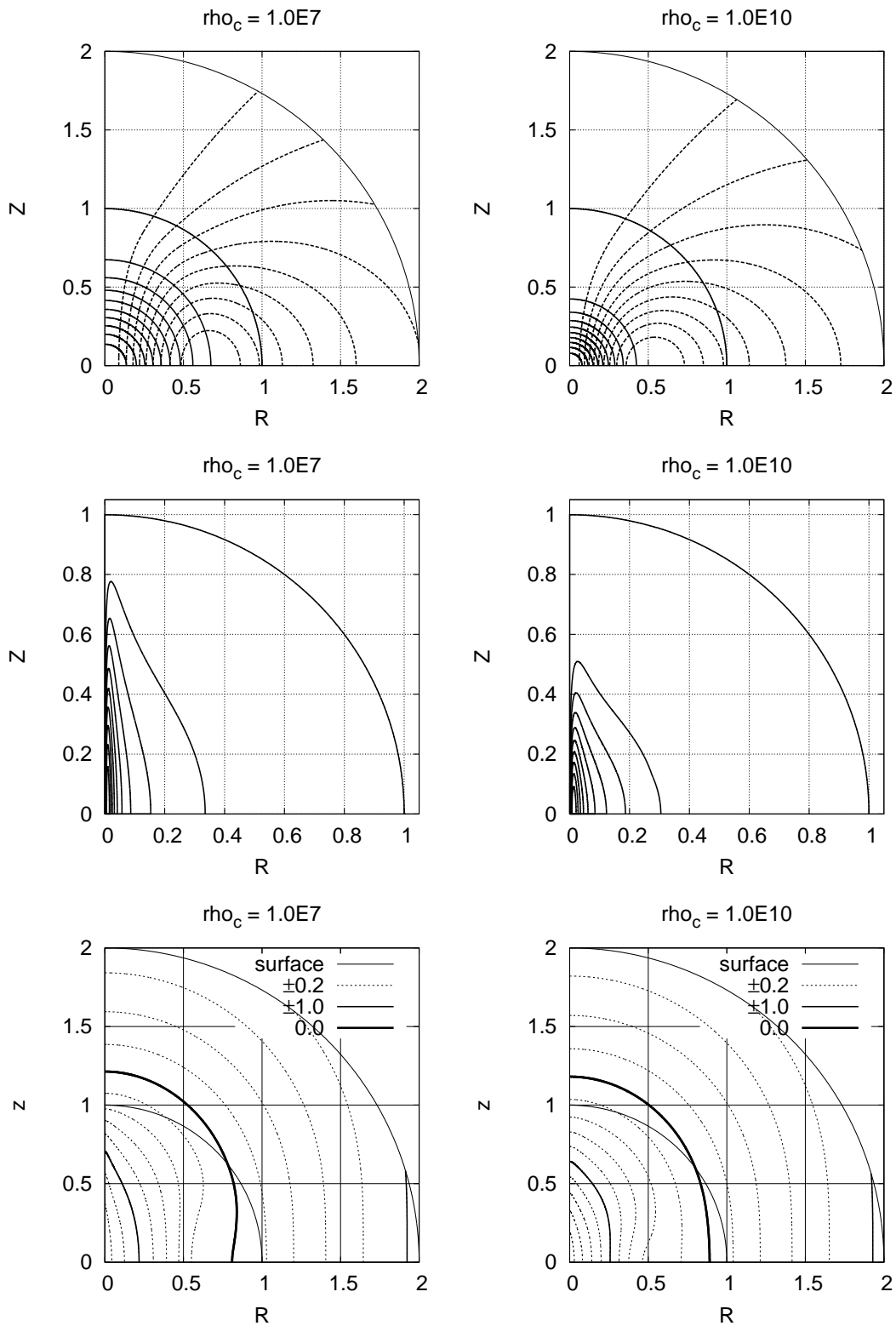


Figure 8. Same as Fig.7 except for the equations of state. The left panels are for a white dwarf with $1.0 \times 10^7 \text{gcm}^{-3}$ and the right panels are for a white dwarf with $1.0 \times 10^{10} \text{gcm}^{-3}$.

beforehand. If one does not have any information about the system to be solved, one has no principle by which to choose the form of the rotation law.

The situation is the same for the *stationary* problem for axisymmetric magnetized *barotropes*. For the stationary states of axisymmetric magnetized barotropes, the situation is more complicated than that for rotating barotropes, because not only the flow velocity but also the magnetic field appears in the problem. That also leads to the appearance of a greater number of arbitrary functions in the problem. Thus it is very hard to specify the forms of arbitrary functions *physically meaningfully*. In such situations the only thing one can might be to explore many kinds of arbitrary functions to find out the general consequences of the resulting magnetic fields.

Of course, if one could obtain a lot of information of the magnetic characteristics about the equilibrium states at hand, one could constrain the arbitrary functions more appropriately and more physically meaningfully. One possibility is to rely on the stability nature of the equilibrium, as in the rotating barotropic stars. Since there is no useful stability criterion for the field configuration with both *poloidal* and *toroidal* fields and linear stability analysis of the equilibrium is beyond our scope, we leave this issue of constraining the functional form for a future study.

4.3 Application to magnetars

The typical strength of the surface magnetic field of anomalous X-ray pulsar (AXP) and soft gamma-ray repeater (SGR) is considered to be $10^{14} - 10^{15}$ G by assuming the magnetic dipole spin down (see e.g. Kouveliotou et al. 1998; Kouveliotou et al. 1999; Murakami et al. 1999; Esposito et al. 2009; Enoto et al. 2009; Enoto et al. 2010). According to recent observational evidences, some types of AXP and SGR are regarded as similar kinds of isolated neutron star and are categorized as magnetars, although they were first considered to belong to two different types of neutron star. (see e.g. Duncan & Thompson 1992; Duncan & Thompson 1996; Woods & Thompson 2006; Mereghetti 2008).

For neutron stars with a strong magnetic field, such as magnetars, the strength of the maximum *toroidal* magnetic field inside has been estimated to be 10^{17} G (see e.g. Thompson & Duncan 1995; Kluźniak & Ruderman 1998; Spruit 1999; Spruit 2009). Many authors have considered that only *toroidal* magnetic fields could become extremely strong and be hidden below the surfaces of the stars. Concerning *poloidal* magnetic fields, a very strong field is not considered because it would be observed as a strong surface field since it is dipole-dominated. However, as shown in this paper, extremely strong *poloidal* magnetic fields can exist in the very central region at $r_c \sim 0.01r_e$, as seen from Tables 1 and 2 and Fig. 6 and the definition of H_c , Equation(39). If we apply our equilibrium models with negative values of m to magnetars with mass $1.4M_\odot$, central density $\rho_{\max} = 1.0 \times 10^{15} \text{ g cm}^{-3}$ and average strength of the surface magnetic fields 10^{15} G, the strengths of the *poloidal* magnetic fields could be $10^{16} - 10^{17}$ G. We also consider weak magnetized magnetars with average strength of the surface magnetic fields 10^{13} G (Rea et al. 2010). If we apply our equilibrium models, the strengths of the *poloidal* magnetic fields

could be $10^{14} - 10^{15}$ G. Since these strong *poloidal* magnetic fields located nearly along the magnetic axis in the central core region, the magnetic structures in the core region are highly anisotropic. If extremely strong magnetic *poloidal* fields are hidden within the core region, there could be magnetic fields with higher order multipole moments.

If the neutron star shape is deformed by a strong magnetic field and the magnetic axis is not aligned the rotational axis, gravitational waves will be emitted (Cutler 2002; Haskell et al. 2008; Mastrano et al. 2011). Gravitational wave emission tends to become stronger as the ellipticity of the meridional plane of the star becomes larger. For our models, decreasing m increases the value of $1 - q$ in the H_{sur} constant sequence (see the value of $1 - q$ in Table 1). Thus those models with highly localized magnetic field here may be efficient emitters of gravitational wave.

4.4 Some features of highly magnetized white dwarfs

It is widely believed that the effect of the stellar magnetic fields play a significant role in astrophysics. For example, isolated magnetized white dwarfs tend to have a higher mass than non-magnetic white dwarfs (Wickramasinghe & Ferrario 2000). According to observations, the surface magnetic field strength of white dwarfs varies from very little to 10^9 G (Wickramasinghe & Ferrario 2000). Therefore, there are some strongly magnetized white dwarfs whose surface magnetic field about 10^8 - 10^9 G. For example, Jordan et al. (1998) estimated the field range 3.0×10^8 - 7.0×10^8 G in GD 299. EUVE J0317-855 is a massive high-field magnetic white dwarf with rapid rotation. Its magnetic field was calculated by an offset dipole model with 4.5×10^8 G and period of 725 s. PG 1031+234 is a high-field magnetized white dwarf. Schmidt et al. (1986) and Latter et al. (1987) estimated its rotation period 3.4 h and its magnetic field as $5.0 \times 10^8 - 1.0 \times 10^9$ G. The observed spectral variations cannot be fitted well by a simple dipole magnetic or offset dipole model, so they have proposed a two-component model composed of a nearly centered dipole and a strongly off-centered dipole. In other words, the magnetic field structures of several strongly magnetized white dwarfs could not be explained by applying simple dipole structures.

We have obtained strongly magnetized white dwarfs with higher order magnetic multipole moments in this paper. If we apply our configurations with negative m , some strongly magnetized star such as PG 1031+234 may have strong interior magnetic fields. According to our numerical results, H_c could reach as high as 10^{12} G when $H_{sur} \sim 3.0 \times 10^9$ G for a highly localized ($m = -3.0$) and high mass ($\rho_c = 1.0 \times 10^9$, $M \sim 1.34M_\odot$) model (see Fig. 6). Since the central magnetic field strength H_c depends on the equation of state as we have shown in Sec.3.3, it becomes higher as the central density increases. Thus high mass white dwarfs could have strong *poloidal* magnetic fields according to our models with negative m . As we have displayed in Sec. 3.1, $N = 1.5$ polytropes with negative values of m have rather large higher order magnetic multipole moments. The same is the case for magnetized white dwarf models, i.e. they have rather large higher order magnetic multipole moments. Therefore, the magnetic fields outside of such stars are far from simple dipole fields if the magnetized

white dwarfs have highly localized strong *poloidal* magnetic fields deep inside the stars.

4.5 Comments on stability of magnetized barotropes

Once equilibrium configurations are obtained, it would be desirable to investigate their stability. However, a satisfactory formulation for the linear stability analysis for general magnetic configurations has not been fully developed, although there is a stability criterion only for purely *toroidal* magnetic configurations (Tayler 1973). For purely *poloidal* or mixed *poloidal-toroidal* magnetic configurations, magnetic configurations with rotation or other general situations, no authors have ever succeeded in obtaining a clear stability criterion (see e.g. Markey & Tayler 1973; Wright 1973; Markey & Tayler 1974; Tayler 1980; Bonanno & Urpin 2008). Therefore the stability of the configurations obtained in this paper contain both *poloidal* and *toroidal* magnetic fields has not been investigated.

By contrast, the stability of magnetized stars may be investigated through that time-dependent evolutionary computations of the magnetic configurations. Thanks to powerful computers, some authors have recently employed magnetohydrodynamical codes to follow the time evolutions of magnetized configurations and find out whether these configurations would settle down to certain 'stable equilibrium states'. Such investigations concerning the magnetic configurations have been carried out by Braithwaite and his coworkers as mentioned in Introduction (see e.g. Braithwaite & Spruit 2004; Braithwaite & Nordlund 2006; Braithwaite & Spruit 2006; Braithwaite 2006; Braithwaite 2007; Braithwaite 2009; Duez et al. 2010). According to their results, purely *toroidal* configurations and purely *poloidal* configurations are shown to be all unstable, as previously shown or expected (e.g. Tayler 1973; Markey & Tayler 1973; Flowers & Ruderman 1977. However, see Geppert & Rheinhardt 2006 for some results about stability). Concerning the mixed *poloidal-toroidal* magnetic configurations, recent numerical studies (Braithwaite 2009; Duez et al. 2010) have shown that they are stable as long as the following condition is satisfied:

$$\alpha_0 \frac{\mathcal{H}}{|W|} \leq \frac{\mathcal{H}_p}{\mathcal{H}} \leq 0.8, \quad (50)$$

where α_0 is a numerical factor of $10 - 10^3$ depending on the stellar structures. By performing 3D MHD simulations, it has been shown that non-axisymmetric perturbations to equilibrium stars grow when this condition is not satisfied. Stars with mixed magnetic fields whose dominant component is *poloidal* field seem to evolve toward non-axisymmetric configurations until the amplitude of the perturbations reach nonlinear regime and saturate. As can be seen from tables in this paper, we have found no models that satisfy that criterion (equation 50) for our particular choice of functional forms presented above (see Sec.2.2), because the energy stored in the *toroidal* magnetic field is at most a few per cent for all of our models. In order to obtain configurations that satisfy the criterion, we need to choose different functional forms from those used in this paper. We should be careful to apply the criterion, however, to general configurations of magnetic fields. The class of solutions with both *toroidal* and *poloidal* magnetic fields obtained

here may be rather different from the ones studied by Braithwaite and his collaborators, even if they share the obvious characteristics of twisted-torus structures of magnetic fields. As is seen in completely different stability natures of seemingly similar configurations in Geppert & Rheinhardt (2006) and Braithwaite (2007), it is quite uncertain at this moment that failure to satisfy the criterion (equation 50) for our models here means unstable nature of them. It would be interesting to study the stability nature of our configurations thorough either linear perturbation analysis or direct MHD simulations.

4.6 Conclusions

In this paper, we have presented an extended formulation for obtaining axisymmetric and stationary barotropic configurations with both the *poloidal* and *toroidal* magnetic fields. We have shown the possibility that magnetized stars have strong *poloidal* magnetic fields inside the star. Our findings and conjectures can be summarized as follows.

- (i) By choosing the functional form for one of the arbitrary functions that appear in the basic formulation for the configurations under the assumptions mentioned before, we have obtained magnetized configurations in which extremely strong *poloidal* fields are confined within the central part of the near axis region. When we apply our models to magnetars, the interior magnetic strength would be 10^{17} G while the surface magnetic strength is $10^{14} - 10^{15}$ G. On the other hand, if we apply our models to magnetized white dwarfs with mass $\sim 1.34M_{\odot}$, the surface field strength would be 10^9 G and H_c reaches 10^{12} G.
- (ii) If stars have extremely strong *poloidal* magnetic fields deep inside, the contours of magnetic field strengths are not spherical but rather column-like shapes as shown in the figures.
- (iii) If stars have extremely strong magnetic fields deep inside, contributions from higher order magnetic multipole moments to the outer fields around the stars cannot be neglected. This implies that if stars have highly localized and extremely strong magnetic fields deep inside, then observations of magnetic fields around the stars could not be explained by the simple dipole models that have been used in most situations.

ACKNOWLEDGMENTS

We would like to thank Dr. R. Takahashi for his discussion while we were extending the formulation of the present paper. KF would like to thank Dr. K. Taniguchi for discussion and comments on this paper. We would also like to thank the anonymous reviewer for useful comments and suggestions that help us to improve this paper. This research was partially supported by the Grant-in-Aid for Scientific Research (C) of Japan Society for the Promotion of Science (20540225) and by Grand-in-Aid for JSPS Fellows.

REFERENCES

- Bocquet M., Bonazzola S., Gourgoulhon E., Novak J., 1995, *A&A*, 301, 757
- Bonanno A., Urpin V., 2008, *A&A*, 477, 35

- Braithwaite J., 2006, *A&A*, 453, 687
 —, 2007, *A&A*, 469, 275
 —, 2008, *MNRAS*, 386, 1947
 —, 2009, *MNRAS*, 397, 763
 Braithwaite J., Nordlund Å., 2006, *A&A*, 450, 1077
 Braithwaite J., Spruit H. C., 2004, *Nature*, 431, 819
 —, 2006, *A&A*, 450, 1097
 Chandrasekhar S., 1939, *An Introduction to the Study of Stellar Structure.*, Chicago Univ. Press, Chicago, IL
 —, 1956, *Proceedings of the National Academy of Science*, 42, 1
 Chandrasekhar S., Fermi E., 1953, *ApJ*, 118, 116
 Chandrasekhar S., Prendergast K. H., 1956, *Proceedings of the National Academy of Science*, 42, 5
 Ciolfi R., Ferrari V., Gualtieri L., Pons J. A., 2009, *MNRAS*, 397, 913
 Cutler C., 2002, *Phys. Rev. D*, 66, 084025
 Duez V., Braithwaite J., Mathis S., 2010, *ApJ*, 724, L34
 Duez V., Mathis S., 2010, *A&A*, 517, A58+
 Duncan R. C., Thompson C., 1992, *ApJ*, 392, L9
 —, 1996, in R. E. Rothschild & R. E. Lingefelter, eds., *AIP Conf. Proc.*, 366, High Velocity Neutron Stars and Gamma-Ray Bursts. Am. Inst. Phys., New York, p. 111
 Enoto T. et al., 2009, *ApJ*, 693, L122
 Enoto T. et al., 2010, *PASJ*, 62, 475
 Esposito P. et al., 2009, *MNRAS*, 399, L44
 Ferraro V. C. A., 1954, *ApJ*, 119, 407
 Flowers E., Ruderman M. A., 1977, *ApJ*, 215, 302
 Geppert U., Rheinhardt M., 2006, *A&A*, 456, 639
 Hachisu I., 1986, *ApJS*, 61, 479
 Haskell B., Samuelsson L., Glampedakis K., Andersson N., 2008, *MNRAS*, 385, 531
 Ioka K., Sasaki M., 2004, *ApJ*, 600, 296
 Jordan S., Schmelcher P., Becken W., Schweizer W., 1998, *A&A*, 336, L33
 Kiuchi K., Yoshida S., 2008, *Phys. Rev. D*, 78, 044045
 Kluźniak W., Ruderman M. A., 1998, *ApJ*, 505, L113
 Kouveliotou C., Dieters S., Strohmayer T., van Paradijs J., Fishman G. J., Meegan C. A., Hurley K., Kommers J., Smith I., Frail D., Murakami T., 1998, *Nature*, 393, 235
 Kouveliotou C., Strohmayer T., Hurley K., van Paradijs J., Finger M. H., Dieters S., Woods P., Thompson C., Duncan R. C., 1999, *ApJ*, 510, L115
 Lander S. K., Jones D. I., 2009, *MNRAS*, 395, 2162
 Latter W. B., Schmidt G. D., Green R. F., 1987, *ApJ*, 320, 308
 Lovelace R. V. E., Mehanian C., Mobarri C. M., Sulkanen M. E., 1986, *ApJS*, 62, 1
 Markey P., Tayler R. J., 1973, *MNRAS*, 163, 77
 —, 1974, *MNRAS*, 168, 505
 Mastrano A., Melatos A., Reisenegger A., Akgün T., 2011, *MNRAS*, 417, 2288
 Mereghetti S., 2008, *Astron Astrophys Rev*, 15, 225
 Micketinac M. J., 1973, *Ap&SS*, 22, 413
 —, 1975, *Ap&SS*, 35, 349
 Murakami T., Kubo S., Shibazaki N., Takeshima T., Yoshida A., Kawai N., 1999, *ApJ*, 510, L119
 Ostriker J. P., Hartwick F. D. A., 1968, *ApJ*, 153, 797
 Otani J., Takahashi R., Eriguchi Y., 2009, *MNRAS*, 396, 2152
 Prendergast K. H., 1956, *ApJ*, 123, 498
 Rea N., Esposito P., Turolla R., Israel G. L., Zane S., Stella L., Mereghetti S., Tiengo A., Götz D., Göğüş E., Kouveliotou C., 2010, *Science*, 330, 944
 Schmidt G. D., Stockman H. S., Grandi S. A., 1986, *ApJ*, 300, 804
 Spruit H. C., 1999, *A&A*, 341, L1
 —, 2009, K. G. Strassmeier, A. G. Kosovichev & J. E. Beckman, eds. *Proc. IAU Symp. 259, Cosmic Magnetic Fields: From Planets, to Stars and Galaxies.* Cambridge Univ. Press, Cambridge, p.61
 Tassoul J. L., 2000, *Stellar Rotation.* Cambridge Univ. Press, New York, p.18
 Tayler R. J., 1973, *MNRAS*, 161, 365
 —, 1980, *MNRAS*, 191, 151
 Thompson C., Duncan R. C., 1995, *MNRAS*, 275, 255
 Tomimura Y., Eriguchi Y., 2005, *MNRAS*, 359, 1117
 Urpin V. A., Ray A., 1994, *MNRAS*, 267, 1000
 Wentzel D. G., 1961, *ApJ*, 133, 170
 Wickramasinghe D. T., Ferrario L., 2000, *PASP*, 112, 873
 Woltjer L., 1959a, *ApJ*, 130, 400
 —, 1959b, *ApJ*, 130, 405
 —, 1960, *ApJ*, 131, 227
 Woods P. M., Thompson C., 2006, in Lewin W., van der Kils M., eds, *Compact Stellar X-ray Sources*, Cambridge Univ. Press, New York, p.547
 Wright G. A. E., 1973, *MNRAS*, 162, 339
 Yoshida S., Eriguchi Y., 2006, *ApJS*, 164, 156
 Yoshida S., Yoshida S., Eriguchi Y., 2006, *ApJ*, 651, 462

APPENDIX A: NUMERICAL METHOD

A1 Dimensionless quantities

In this paper, physical quantities are used in their dimensionless forms as follows:

$$\hat{\phi}_g \equiv \frac{\phi_g}{4\pi G r_e^2 \rho_{\max}}, \quad (\text{A1})$$

$$\hat{\Omega} \equiv \frac{\Omega}{\sqrt{4\pi G \rho_{\max}}}, \quad (\text{A2})$$

$$\hat{\kappa} \equiv \frac{\kappa}{\sqrt{4\pi G r_e^2 \rho_{\max}}}, \quad (\text{A3})$$

$$\hat{\mu} \equiv \frac{\mu}{\sqrt{4\pi G}/r_e}, \quad (\text{A4})$$

$$\hat{H}_{\text{suffix}} \equiv \frac{H_{\text{suffix}}}{\sqrt{4\pi G r_e \rho_{\max}}}, \quad (\text{A5})$$

$$\hat{A}_\varphi \equiv \frac{A_\varphi}{\sqrt{4\pi G r_e^2 \rho_{\max}}}, \quad (\text{A6})$$

$$\hat{\Psi} \equiv \frac{\Psi}{\sqrt{4\pi G r_e^3 \rho_{\max}}}, \quad (\text{A7})$$

$$\hat{K} \equiv \frac{K}{4\pi G r_e^6 \rho_{\max}^2}, \quad (\text{A8})$$

$$\hat{j}_\varphi \equiv \frac{j_\varphi}{\sqrt{4\pi G r_e^2 \rho_{\max} c}}. \quad (\text{A9})$$

$$\hat{C} \equiv \frac{C}{4\pi G r_e^2 \rho_{\max}}. \quad (\text{A10})$$

Here H_{suffix} is the component of the magnetic field where *suffix* may be *c* (center), *sur* (surface), *p* (*poloidal*) and *t* (*toroidal*). Similarly we define normalized global quantities as follows:

$$\hat{M} = \frac{M}{r_e^3 \rho_{\max}}, \quad (\text{A11})$$

$$\hat{W} = \frac{W}{4\pi G r_e^5 \rho_{\max}^2}, \quad (\text{A12})$$

$$\hat{T} = \frac{T}{4\pi G r_e^5 \rho_{\max}^2}, \quad (\text{A13})$$

$$\hat{\Pi} = \frac{\Pi}{4\pi G r_e^5 \rho_{\max}^2}, \quad (\text{A14})$$

$$\hat{U} = \frac{U}{4\pi G r_e^5 \rho_{\max}^2}, \quad (\text{A15})$$

$$\hat{\mathcal{H}} = \frac{\mathcal{H}}{4\pi G r_e^5 \rho_{\max}^2}. \quad (\text{A16})$$

We also define dimensionless forms of arbitrary functions as follows:

$$\hat{\kappa}(\hat{\Psi}) = \begin{cases} 0, & \text{for } \hat{\Psi} \leq \hat{\Psi}_{\max}, \\ \frac{\hat{\kappa}_0}{k+1} (\hat{\Psi} - \hat{\Psi}_{\max})^{k+1}, & \text{for } \hat{\Psi} \geq \hat{\Psi}_{\max}, \end{cases} \quad (\text{A17})$$

$$\frac{d\hat{\kappa}(\hat{\Psi})}{d\hat{\Psi}} = \begin{cases} 0, & \text{for } \hat{\Psi} \leq \hat{\Psi}_{\max}, \\ \hat{\kappa}_0 (\hat{\Psi} - \hat{\Psi}_{\max})^k, & \text{for } \hat{\Psi} \geq \hat{\Psi}_{\max}. \end{cases} \quad (\text{A18})$$

for κ and

$$\hat{\mu}(\hat{\Psi}) = \hat{\mu}_0 (\hat{\Psi} + \hat{\epsilon})^m, \quad (\text{A19})$$

$$\int \hat{\mu}(\hat{\Psi}) d\hat{\Psi} = \frac{\hat{\mu}_0}{m+1} (\hat{\Psi} + \hat{\epsilon})^{m+1}. \quad (\text{A20})$$

for μ . We choose $k = 0.1$, $\hat{\kappa}_0 = 10$ and $\hat{\epsilon} = 1.0 \times 10^{-6}$ and keep their values fixed during all calculations in this paper.

A2 Computational grids

We describe the details of our numerical grid points. In order to resolve the distributions of the source term of the vector potential equation without loss of accuracy, we choose the following non-uniformly distributed grid points in the actual numerical computations. In the \hat{r} -direction, we divide the whole space into two distinct regions: $[0, 1.0]$ (region 1), and $[1.0, 2.0]$ (region 2). In each region, the following mesh points are defined:

$$\hat{r}_i = w_i^2 \begin{cases} w_i = (i-1)\Delta w_1, & \Delta w_1 \equiv \frac{\sqrt{1}-\sqrt{0}}{n_1-1}, & \text{for } 1 \leq i \leq n_1, \\ w_i = 1.0 + (i-n_1)\Delta w_2, & \Delta w_2 \equiv \frac{\sqrt{2}-\sqrt{1}}{n_2-1}, & \text{for } n_1 \leq i. \end{cases} \quad (\text{A21})$$

where n_1 and n_2 are the mesh numbers defined as follows:

$$n_1 \equiv \frac{3}{4}(n_r - 1) + 1, \quad (\text{A22})$$

$$n_2 \equiv \frac{1}{4}(n_r - 1) + 1. \quad (\text{A23})$$

Here n_r is the total mesh number in the r -direction. In practice, since we use a difference scheme of the second-order accuracy for the derivative and Simpson's integration formula, we divide each mesh interval defined above further into two equal size intervals in the r coordinate. We use $n_r = 513$ and thus the actual total number of the mesh points is $(2n_r - 1) = 1025$.

Concerning the θ -direction, we have to resolve the region near the axis, because for $m < 0$ values the magnetic fields seem to be highly localized to the axis region. In order to treat such magnetic fields near the axis region, we introduce the following mesh in the θ -direction:

$$\theta_j = \lambda_j^2, \quad \lambda_j = (j-1)\Delta\lambda, \quad 1 \leq j \leq n_\theta, \quad \Delta\lambda = \frac{\sqrt{\pi/2}}{n_\theta - 1} \quad (\text{A24})$$

where n_θ is the total mesh number in the θ -direction. We also divide each mesh interval defined above further into two equal size intervals. Then, we use $n_\theta = 513$ and thus the actual total number of the mesh points is 1025. Fig. A1 shows the relations between the order of the grid points and the r - or θ -coordinate value.

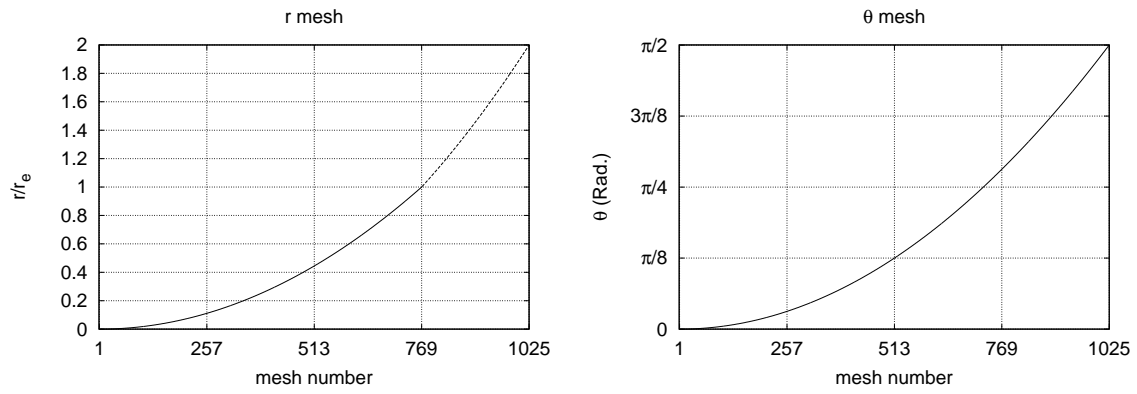


Figure A1. Left: the coordinate r/r_e is plotted as a function of the grid points. The solid curve shows the region 1 ($[0, 1]$) and the dashed curve shows the region 2 ($[1, 2]$). Right: the same as the left panel except for the θ coordinate.